The high-pressure phase of alumina and implications for Earth's D″ layer

Artem R. Oganov*† and Shigeaki Ono‡

*Laboratory of Crystallography, Department of Materials, Eidgenössische Technische Hochschule Hönggerberg, HCI G 515, Wolfgang-Pauli-Strasse 10, CH-8093 Zurich, Switzerland; and ‡Institute for Research on Earth Evolution, Japan Agency for Marine-Earth Science and Technology, 2-15 Natsushima-cho, Yokosuka-shi, Kanagawa 237-0061, Japan

Edited by David J. Stevenson, California Institute of Technology, Pasadena, CA, and approved June 7, 2005 (received for review March 4, 2005)

Using *ab initio* simulations and high-pressure experiments in a diamond anvil cell, we show that alumina (Al_2O_3) adopts the $CaIrO_3$-type structure above 130 GPa. This finding substantially changes the picture of high-pressure behavior of alumina; in particular, we find that perovskite structure is never stable for Al_2O_3 at zero Kelvin. The $CaIrO_3$-type phase suggests a reinterpretation of previous shock-wave experiments and has important implications for the use of alumina as a window material in shock-wave experiments. In particular, the conditions of the stability of this phase correspond to those at which shock-wave experiments indicated an increase of the electrical conductivity. If this increase is caused by high ionic mobility in the $CaIrO_3$-type phase of Al_2O_3, similar effect can be expected in the isostructural postperovskite phase of $MgSiO_3$ (which is the dominant mineral phase in the Earth's D″ layer). The effect of the incorporation of Al on the perovskite/postperovskite transition of $MgSiO_3$ is discussed.

ab initio | $CaIrO_3$ type | Al_2O_3 | phase diagram | density-functional perturbation theory

Alumina (Al_2O_3) is an important ceramic material and a major chemical component of the Earth. High-pressure behavior of alumina is an issue of paramount importance for three reasons: (*i*) static compression experiments often rely on the ruby pressure scale (1), (*ii*) alumina is used as an optical window material in shock-wave experiments, and its properties (e.g., the electrical conductivity) will affect measurements, and (*iii*) alumina, although unlikely as an individual mineral phase in the Earth's mantle, is incorporated into mantle minerals and significantly affects their physical properties (e.g., refs. 2 and 3).

According to theoretical (e.g., refs. 4–6) and experimental (7–9) studies, at high pressures corundum transforms into the Rh_2O_3(II)-type structure. This well established transition, occurring at 80–100 GPa (5–9), implies that the ruby pressure scale should not be used above ≈80 GPa in experiments that involve heating to temperatures where this phase transition will be kinetically feasible. Less clear evidence exists for a further transition. Lin *et al.* (9) reported that Rh_2O_3(II) structure is stable at least up to 130 GPa and 2,000 K, but above 130 GPa (at temperatures ≈1,500 K) shock-wave experiments of Weir *et al.* (10) indicated onset of an increase in the electrical conductivity that could be caused by a phase transition. Shock-wave Hugoniots of Al_2O_3 compiled by Hama and Suito (11) also give evidence for a possible phase transition at 130 GPa with a small increase of density. Thomson *et al.* (6) predicted that an orthorhombic (*Pbnm*) perovskite structure becomes more stable than Rh_2O_3(II), but only above 200 GPa. The discovery of postperovskite $CaIrO_3$-type polymorphs of Fe_2O_3 (12) and $MgSiO_3$ (13, 14) prompts the question of whether a similar phase exists for Al_2O_3.

In our *ab initio* calculations, we consider four Al_2O_3 polymorphs: corundum (space group $R\bar{3}c$), Rh_2O_3(II) (*Pbcn*), perovskite (*Pbnm*), and $CaIrO_3$-type (*Cmcm*). Our calculations are based on the plane wave pseudopotential methodology and the local density approximation (LDA) as implemented in the ABINIT code (15), a common project of the Université Catholique de Louvain (Louvain, Belgium), Corning, and other contributors (www.abinit.org). The pseudopotentials used are of the Troullier-Martins (16) type, fully nonlocal and including partial core corrections (17); the core radii are 0.766 Å for O ($1s^2$ core) and 1.204 Å for Al ($1s^22s^22p^6$ core). The plane wave kinetic energy cut-off of 45 Ha enabled convergence to within 12 meV per atom for the total energy, 0.06 meV per atom for the energy differences, and within 0.6 GPa for pressure. The Monkhorst-Pack meshes used for sampling of the Brillouin zone were $4 \times 4 \times 4$ for Rh_2O_3(II) and perovskite structures, $6 \times 6 \times 6$ for corundum structure, and $6 \times 6 \times 4$ for $CaIrO_3$-type phase (for the latter two phases primitive 10-atom cells were used in all calculations). The dynamical matrices were calculated by using density-functional perturbation theory (18) on $2 \times 2 \times 2$ reciprocal space grids for Rh_2O_3(II) and perovskite structures, $3 \times 3 \times 3$ for corundum, and $3 \times 3 \times 2$ for $CaIrO_3$-type phase. These, together with the computed values of the dielectric constants and Born effective charges, allowed for an accurate interpolation of the dynamical matrices throughout the Brillouin zone and the calculation of phonon densities of states and thermodynamic properties within the quasiharmonic approximation. For more methodological details, see refs. 13 and 19–21.

Let us first analyze results of calculations at 0 K. Parameters of the Vinet equation of state (22) for different phases of alumina are given in Table 1. One can notice good agreement with available experimental data at room temperature (23) and previous calculations (6). Fig. 1*a* shows the calculated static enthalpy differences between phases. The transition from corundum to the Rh_2O_3(II) structure is predicted to occur at 80 GPa, similar to previous calculations (5, 6) and experiment (7–9). At 131 GPa we predict a transition from the Rh_2O_3(II) structure to the $CaIrO_3$-type phase; perovskite structure is never stable at 0 K. It is well known that the LDA usually underestimates phase transition pressures, whereas the generalized gradient approximation tends to slightly overestimate these pressures (24). To evaluate possible errors coming from the LDA and the pseudopotentials, we performed calculations within the generalized gradient approximation (25) by using the all-electron projector-augmented wave method (26) as implemented in the VASP code (27). Projector-augmented wave potentials had [He] core (radius 1.52 a.u.) for O and [Ne] core (1.90 a.u.) for Al; we used 600-eV plane-wave cutoff and 2,400-eV cutoff for the augmentation charges. The results were similar to the LDA calculations, with pressures of 92 and 147 GPa for the corundum-Rh_2O_3(II) and Rh_2O_3(II)-$CaIrO_3$ transitions, respectively. Thus we estimate that our LDA predictions of phase transition pressures are likely to be shifted by

This paper was submitted directly (Track II) to the PNAS office.

Abbreviation: LDA, local density approximation.

†To whom correspondence should be addressed. E-mail: a.oganov@mat.ethz.ch.

www.pnas.org/cgi/doi/10.1073/pnas.0501800102

Table 1. Equation of state parameters for Al_2O_3 phases (per formula unit)

Phase	E_0, eV	V_0, Å^3	K_0, GPa	K_0'	Source
Corundum	0.0	42.428	252.6	4.237	This work (theory)
	–	42.20	258.9	4.01	Ref. 6 (theory)
	–	42.42	254.4	4.275	Ref. 23 (experiment)
Rh_2O_3(II)	0.422	41.422	258.2	4.140	This work (theory)
	0.4	41.27	261.8	3.93	Ref. 6 (theory)
Perovskite	0.807	41.618	229.2	4.286	This work (theory)
	0.75	41.61	235.0	3.98	Ref. 6 (theory)
$CaIrO_3$	1.322	40.292	241.6	4.464	This work (theory)

E_0, V_0, K_0, K_0' are the energy (relative to corundum), volume, bulk modulus, and its pressure derivative, respectively, at zero pressure.

≈10–15 GPa toward lower pressures. The existence of a $CaIrO_3$-type phase of alumina is supported by static pseudopotential calculations (28). However, significantly higher transition pressures were reported in ref. 28, with the LDA (generalized gradient approximation) values of 105 (100) GPa and 156 (153) GPa for the corundum-Rh_2O_3(II) and Rh_2O_3(II)-$CaIrO_3$ transitions, respectively. This difference could be caused by the pseudopotentials used in ref. 28.

Our calculated phase diagram (Fig. 1*b*) shows that both corundum-Rh_2O_3(II) and Rh_2O_3(II)-$CaIrO_3$ transitions have negative Clapeyron slopes. Taking into account these slopes and the ≈10–15 GPa underestimation of the LDA transition pressures, the agreement between the shock-wave phase transition point (≈130 GPa at 1,000–1,500 K) and our predicted Rh_2O_3(II)-$CaIrO_3$ transition pressure (119 GPa at 1,500 K) is excellent. We believe that Lin *et al.* (9) did not observe this transition because pressures a few GPa higher than those achieved in their study (up to 130 GPa at high temperature) are needed to produce this transition; also, the uncertainty of pressure calibration at such pressures and temperatures is ≈10%. We tentatively ascribe the change of the electrical conductivity of Al_2O_3 at 130 GPa (10) to this phase transition. To explore this idea further, we have performed *ab initio* molecular dynamics simulations at ≈150 GPa and 5,000 K, in the *NVT*-ensemble (29) for a 120-atom supercell. These simulations were based on the generalized gradient approximation and projector-augmented wave method and were done by using VASP, with the Γ-point for Brillouin zone sampling and 500-eV plane-wave kinetic energy cut-off. Because of a relatively short duration of these simulations (1.5 ps) we could not observe diffusion, even when oxygen vacancies were introduced. Yet, there are hints that diffusion would take place on longer time scales: we observed very vigorous and highly anisotropic motion of O atoms, especially in the presence of vacancies. The high electrical conductivity of this phase (2 S/m at 155 GPa and below 2,000 K) observed by Weir *et al.* (10) suggests that an isostructural postperovskite phase of $MgSiO_3$, the main mineral of the Earth's D″ layer (13, 14, 30, 31), could also possess high conductivity (which will rapidly increase with temperature) associated with diffusion of the O^{2-} ions. There are other possible explanations of the electrical conductivity of the D″ layer (32), e.g., a chemical reaction between the core and mantle producing metallic Fe-Si alloys and/or FeO (e.g., refs. 33 and 34). Note that there may be a nonnegligible electronic component in the electrical conductivity of postperovskite $MgSiO_3$, because this phase is expected to contain significant amounts of Fe^{2+} and Fe^{3+} in the Earth's mantle (13, 30, 31).

From Fig. 1*b* one can also see that perovskite phase, because of its higher entropy, may become stable at high temperatures and ≈100 GPa. However, we note that at corresponding volumes perovskite is dynamically unstable (i.e., has soft modes), and its stability field was calculated on the basis of extrapolation of thermodynamic properties from pressures above 130 GPa, where it has no soft modes. Although anharmonic effects often suppress dynamical instabilities at high temperatures and may justify such an extrapolation, the calculated stability field of perovskite phase should be treated with caution: there may, in fact, be another phase stable in that region of *P-T* space. The dynamical instability arises from the fact that at low pressures Al^{3+} ions are too small for the 8-fold coordinated sites in perovskite and $CaIrO_3$ structure. $CaIrO_3$-type alumina is dynamically unstable below ≈50 GPa, i.e., it cannot be quenched below 50 GPa and has to be observed *in situ*.

We have also been able to confirm the stability of $CaIrO_3$-type phase of Al_2O_3 predicted above by using high-pressure experiments with the laser-heated diamond-anvil cell. A sym-

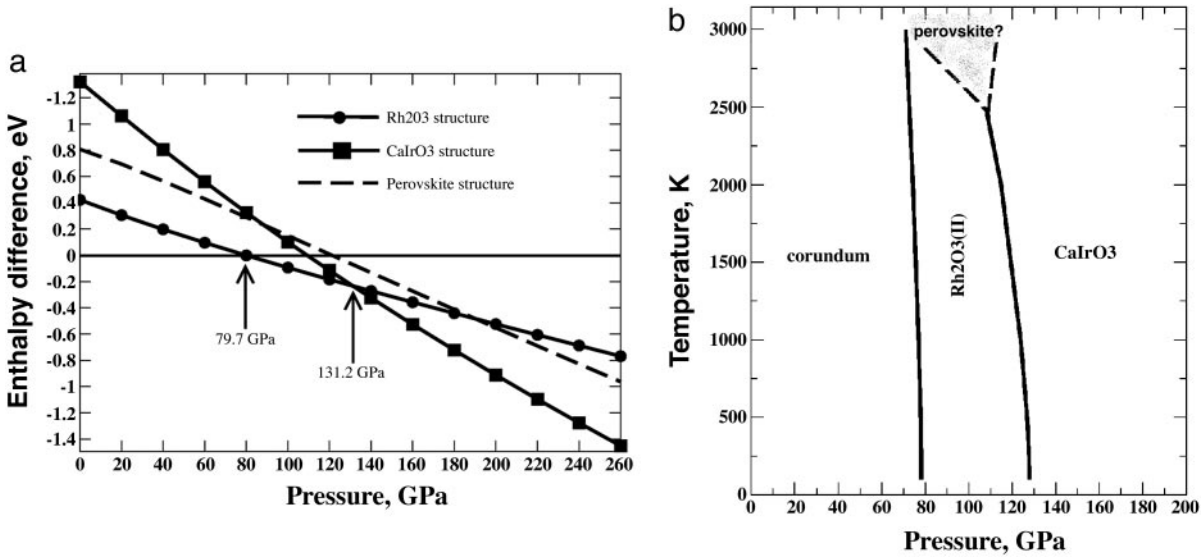

Fig. 1. Structural stability of Al_2O_3. (*a*) Static enthalpies relative to corundum. (*b*) Phase diagram. Hatched area with dashed boundaries corresponds to a possible stability field of Al_2O_3-perovskite.

metric-type diamond cell with 50° conical apertures was used (35). To avoid problems caused by metastability, we decided to conduct experiments at pressures much higher than 130 GPa. Powdered Al_2O_3 was loaded into 50-μm holes drilled in rhenium gaskets. No pressure-transmitting medium was used in this study. Gold powder was mixed with the sample to provide an internal pressure calibrant and an absorber of laser heating. The efficiency of laser absorbance for gold was sufficiently high to heat the sample. The samples were heated with a TEM_{01}-mode Nd:YLF laser using double-sided laser heating techniques that minimized temperature gradients (both axial and radial) of the heated area. The size of the heating spot was ≈20–30 μm. The sample temperature was measured from both sides by using the spectroradiometric method. The heated samples were probed by angle-dispersive x-ray diffraction using the synchrotron beam line BL10XU at SPring-8 in Hyogo, Japan. The incident x-ray beam was monochromatized to a wavelength of 0.4145 Å. The x-ray beam size was collimated to 15 μm diameter. Alignment of the x-ray and laser spots can be achieved within 5 μm. Angle-dispersive x-ray diffraction patterns were obtained on an imaging plate. The distances between the sample and the detectors were measured by using CeO_2 as a standard. The observed intensities on the imaging plate were integrated as a function of 2θ to give conventional, 1D diffraction profiles. Experimental details have been described elsewhere (36). Pressure was determined from the measured unit cell volume of gold (37). It is known that several equations of state of gold have been reported, and there is a significant discrepancy among them. The uncertainty of pressure associated with the equation of state for gold was ≈10%. Initially, the sample was compressed to ≈170 GPa at room temperature, where the stability field of $CaIrO_3$-type phase was expected from calculations. However, no diffraction peaks of $CaIrO_3$-type phase of Al_2O_3 could be identified. After the desired pressure was achieved, the sample was heated to ≈2,500 K to overcome potential kinetic effects on possible phase transition. During the heating, new diffraction peaks appeared at 200 GPa and 2,500 K. After quenching to 163 GPa and 300 K, these diffraction peaks remained stable. The decrease of sample pressure was likely caused by effects of the thermal expansion and the stress relaxation during laser heating. All of the diffraction peaks were reasonably well indexed by the $CaIrO_3$-type structure (Fig. 2). Other peaks belonged to the gold internal pressure calibrant and the rhenium gasket. These experimental results agreed with the predicted phase diagram of Al_2O_3 (Fig. 1).

To clarify the effect of Al incorporation on the postperovskite phase transition in $MgSiO_3$, we have considered the coupled Al-Al substitution in perovskite and postperovskite phases of $MgSiO_3$ according to reactions

$$MgSiO_3 + xAl_2O_3 = (Mg_{1-x}Al_x)(Si_{1-x}Al_x)O_3 + xMgSiO_3$$

for both structures. The most interesting quantity, namely the enthalpy difference for Al substitutions in perovskite and postperovskite, plotted in Fig. 3, shows that Al strongly prefers to enter $MgSiO_3$ perovskite. The effect of 5 mol% concentration of Al_2O_3 in $MgSiO_3$ is to increase the postperovskite transition pressure by 5.2 GPa, much more than ≈1 GPa predicted in ref. 28 on the basis of a simple linear extrapolation between the end members. However, Fe^{2+} and Fe^{3+} impurities more than cancel this effect: e.g., according to our calculations (30), 10 mol% incorporation of FeO would decrease this pressure by 8.7 GPa [or by ≈10 GPa from experiments (31)], the result being that for natural mantle compositions the postperovskite transition pressure is a few GPa lower than for pure $MgSiO_3$ (30). This finding supports the original suggestions (13, 14) that the postperovskite phase of $MgSiO_3$ with the $CaIrO_3$-type structure is the main mineral of the Earth's D″ layer.

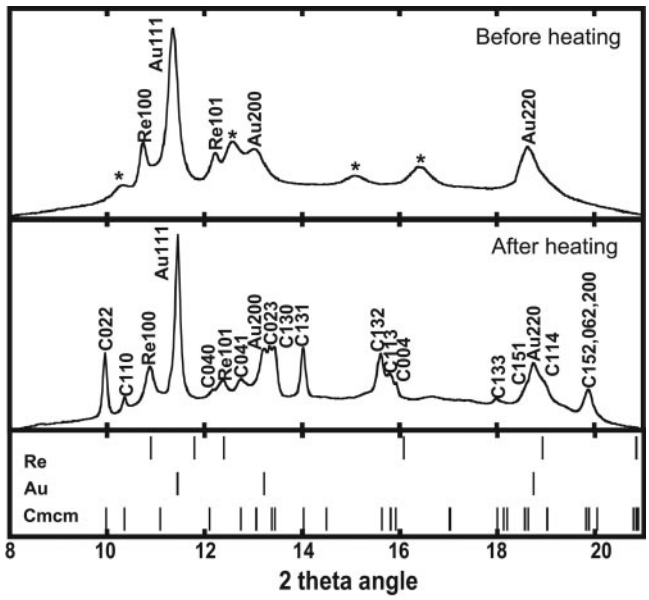

Fig. 2. Experimental powder diffraction pattern at 163 GPa and 300 K. Cmcm, $CaIrO_3$-type Al_2O_3 phase; Au, gold used as an internal pressure calibrant; Re, rhenium of the gasket; *, broad peaks from the sample before transition. Observed unit cell dimensions of $CaIrO_3$-type Al_2O_3 phase are a = 2.402(2) Å, b = 7.863(5) Å, c = 5.989(5) Å, V = 113.12(14) Å^3. The corresponding theoretical values are a = 2.420 Å, b = 7.920 Å, c = 6.037 Å, V = 115.68 Å^3. Vertical bars indicate the calculated positions of the diffraction lines of each phase.

Earlier, we found that phase (13) based on the observation of an analogous phase in Fe_2O_3 (12). We believe that studies of analogous materials (such as Al_2O_3, Fe_2O_3, $NaMgF_3$, and $CaTiO_3$) will continue to provide important insight into the properties of the Earth's lowermost mantle and set interesting physical questions. In particular, the nature of high-pressure stability of the $CaIrO_3$-type phases with their layered structure originally came as a surprise (12–14) and still remains enigmatic. It is unclear why some analogous materials adopt this structure at high pressure (e.g., Fe_2O_3, $MgSiO_3$, Al_2O_3), whereas others do not [e.g., $CaSiO_3$ (38)].

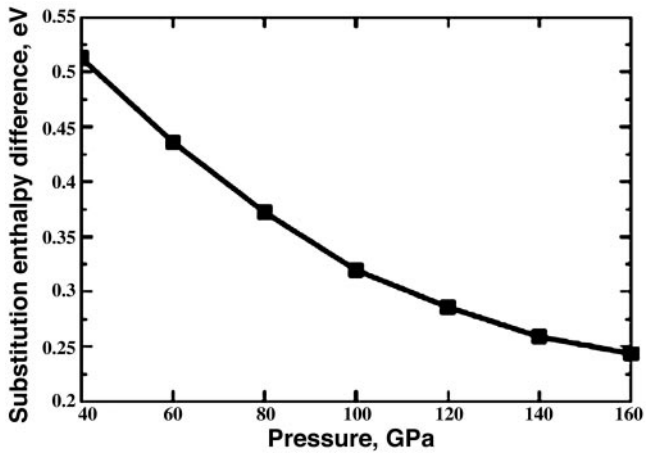

Fig. 3. Al-Al coupled substitution enthalpy difference between perovskite and postperovskite. Positive values indicate greater solubility of Al_2O_3 in perovskite.

We thank T. Koyama, N. Sata, and Y. Ohishi for fruitful discussion and experimental help. Calculations were performed at the Eidgenössische Technische Hochschule Zurich and the Swiss National Supercomputing Centre (Manno). The synchrotron radiation experiments were performed at the high-pressure research beamline BL10XU, SPring-8 (Proposal 2003A0013-LD2-np).

1. Mao, H. K., Xu, J. & Bell, P. M. (1986) *J. Geophys. Res.* **91,** 4673–4676.
2. Wood, B. J. & Rubie, D. C. (1996) *Science* **273,** 1522–1524.
3. Zhang, J. Z. & Weidner, D. J. (1999) *Science* **284,** 782–784.
4. Cynn, H., Isaak, D. G., Cohen, R. E., Nicol, M. F. & Anderson, O. L. (1990) *Am. Mineral.* **75,** 439–442.
5. Marton, F. C. & Cohen, R. E. (1994) *Am. Mineral.* **79,** 789–792.
6. Thomson, K. T., Wentzcovitch, R. M. & Bukowinski, M. S. T. (1996) *Science* **274,** 1880–1882.
7. Funamori, N. & Jeanloz, R. (1997) *Science* **278,** 1109–1111.
8. Mashimo, T., Tsumoto, K., Nakamura, K., Noguchi, Y., Fukuoka, K. & Syono, Y. (2000) *Geophys. Res. Lett.* **27,** 2021–2024.
9. Lin, J. F., Degtyareva, O., Prewitt, C. T., Dera, P., Sata, N., Gregoryanz, E., Mao, H. K. & Hemley, R. J. (2004) *Nat. Mater.* **3,** 389–393.
10. Weir, S. T., Mitchell, A. C. & Nellis, W. J. (1996) *J. Appl. Phys.* **80,** 1522–1525.
11. Hama, J. & Suito, K. (2002) *High Temp. High Pres.* **34,** 323–334.
12. Ono, S., Kikegawa, T. & Ohishi, Y. (2004) *J. Phys. Chem. Solids* **65,** 1527–1530.
13. Oganov, A. R. & Ono, S. (2004) *Nature* **430,** 445–448.
14. Murakami, M., Hirose, K., Kawamura, K., Sata, N. & Ohishi, Y. (2004) *Science* **304,** 855–858.
15. Gonze, X., Beuken, J.-M., Caracas, R., Detraux, F., Fuchs, M., Rignanese, G.-M., Sindic, L., Verstraete, M., Zerah, G., Jollet, F., *et al.* (2002) *Comp. Mater. Sci.* **25,** 478–492.
16. Troullier, N. & Martins, J. L. (1991) *Phys. Rev. B* **43,** 1993–2006.
17. Louie, S. G., Froyen, S. & Cohen, M. L. (1982) *Phys. Rev. B* **26,** 1738–1742.
18. Baroni, S., de Gironcoli, S., Dal Corso, A. & Gianozzi, P. (2001) *Rev. Mod. Phys.* **73,** 515–562.
19. Oganov, A. R., Gillan, M. J. & Price, G. D. (2003) *J. Chem. Phys.* **118,** 10174–10182.
20. Oganov, A. R., Gillan, M. J. & Price, G. D. (2005) *Phys. Rev. B* **71,** 064104.
21. Oganov, A. R. & Price, G. D. (2005) *J. Chem. Phys.* **122,** 124501.
22. Vinet, P., Rose, J. H., Ferrante, J. & Smith, J. R. (1989) *J. Phys. Condens. Matter* **1,** 1941–1963.
23. d'Amour, H., Schiferl, D., Denner, W., Schulz, H. & Holzapfel, W. B. (1978) *J. Appl. Phys.* **49,** 4411–4416.
24. Zupan, A., Blaha, P., Schwarz, K. & Perdew, J. P. (1998) *Phys. Rev. B* **58,** 11266–11272.
25. Perdew, J. P., Burke, K. & Ernzerhof, M. (1996) *Phys. Rev. Lett.* **77,** 3865–3868.
26. Kresse, G. & Joubert, D. (1999) *Phys. Rev. B* **59,** 1758–1775.
27. Kresse, G. & Furthmüller, J. (1996) *Phys. Rev. B* **54,** 11169–11186.
28. Caracas, R. & Cohen, R. E. (2005) *Geophys. Res. Lett.* **32,** L06303.
29. Nosé, S. (1984) *Mol. Phys.* **52,** 255–268.
30. Ono, S., Oganov, A. R. & Ohishi, Y. (2005) *Earth Planet. Sci. Lett.*, in press.
31. Mao, W. L., Shen, G., Prakapenka, V. B., Meng, Y., Campbel, A. J., Heinz, D. L., Shu, J., Hemley, R. J. & Mao, H.-K. (2004) *Proc. Natl. Acad. Sci. USA* **101,** 15867–15869.
32. Constable, S. & Constable, C. (2004) *Geochem. Geophys. Geosys.* **5,** Q01006.
33. Dubrovinsky, L., Dubrovinskaia, N., Langenhorst, F., Dobson, D., Rubie, D., Gessmann, C., Abrikosov, I. A., Johansson, B., Baykov, V. I., Vitos, L., *et al.* (2003) *Nature* **422,** 58–61.
34. Jeanloz, R. & Lay, T. (1993) *Sci. Am.* **268,** 48–55.
35. Ono, S., Kikegawa, T. & Ohishi, Y. (2005) *Solid State Commun.* **133,** 55–59.
36. Ono, S., Ohishi, Y., Isshiki, M. & Watanuki, T. (2005) *J. Geophys. Res.* **110,** B02208.
37. Jamieson, J. C., Fritz, J. N. & Manghnani, M. H. (1982) in *High-Pressure Research in Geophysics*, eds. Akimoto, S. & Manghnani, M. H. (Center for Academic Publishing, Tokyo), pp. 27–48.
38. Jung, D. Y. & Oganov, A. R. (2005) *Phys. Chem. Minerals* **32,** 146–153.